Heliyon 10 (2024) e38305

Contents lists available at ScienceDirect

Heliyon

journal homepage: www.cell.com/heliyon

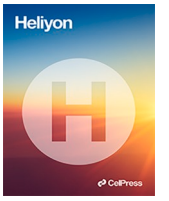

Research article

Structural insight into the lead identification of a dual inhibitor of PDE1B and PDE10A: Integrating pharmacophore-based virtual screening, molecular docking, and structure-activity-relationship approaches

Ching Wen Soon [a], Anand Gaurav [b,c,**], Vertika Gautam [d], Mayasah Al-Nema [a,e,*]

[a] Faculty of Pharmaceutical Sciences, UCSI University, Taman Connaught, Cheras, Kuala Lumpur, 56000, Malaysia
[b] Department of Pharmaceutical Sciences, School of Health Sciences and Technology, UPES, Dehradun, 248007, Uttarakhand, India
[c] Faculty of Health Sciences, Villa College, Male', 20373, Maldives
[d] Institute of Pharmaceutical Research, GLA University, Mathura, 281406, Uttar Pradesh, India
[e] Klarity, Westbourne, Bournemouth, BH4 8DT, United Kingdom

ARTICLE INFO

Keywords:
Schizophrenia
PDE1B
PDE10A
Pharmacophore modelling
Virtual screening
Molecular docking

ABSTRACT

Schizophrenia is a chronic neuropsychiatric disorder affecting more than 1% of the world's population. Current antipsychotic treatments show inadequacy in mitigating the negative and cognitive symptoms of schizophrenia. In addition, these medications cause undesirable extrapyramidal side effects. According to the studies, inhibition of phosphodiesterase (PDE) 1B and PDE10A simultaneously can alleviate positive, negative, and cognitive symptoms of schizophrenia. Thus, this study aims to identify new dual inhibitors of PDE1B and PDE10A using ligand-based pharmacophore modelling, virtual screening, and molecular docking studies. Accordingly, the generated pharmacophore models of PDE1B and PDE10A comprised hydrogen bond acceptor, aromatic ring, and hydrophobic features. These features were essential for retrieving the active hits from the Universal Natural Product Database in the virtual screening. Additional filters were subsequently employed to identify potential hits that could be developed into central nervous system-active compounds. Hits meeting all the screening criteria were subjected to docking studies with PDE1B and PDE10A. Among these hits, UNPD167314 exhibited significant binding affinities for the target receptors. It occupied the P-clamp and displayed hydrophobic, aromatic, and hydrogen bond interactions with the active site residues of both receptors, thus selected as a lead compound for the design of potent and selective dual inhibitors. The structural modifications of UNPD167314 resulted in the design of 35 novel inhibitors. Out of 35, four compounds exhibited high and comparable binding affinities for both PDE1B and PDE10A, making them promising candidates for further evaluation and optimisation.

* Corresponding author. Klarity, Westbourne, Bournemouth, BH4 8DT, United Kingdom.
** Corresponding author. Department of Pharmaceutical Sciences, School of Health Sciences and Technology, UPES, Dehradun 248007, Uttarakhand, India.
E-mail addresses: anand.pharma@gmail.com (A. Gaurav), mayasahalnema@gmail.com (M. Al-Nema).

https://doi.org/10.1016/j.heliyon.2024.e38305
Received 18 December 2023; Received in revised form 5 September 2024; Accepted 22 September 2024
Available online 23 September 2024

1. Introduction

Neuropsychiatric disorders, such as schizophrenia, major depressive disorder, and bipolar disorder, are debilitating illnesses that disrupt the patients' daily activities by altering their perceptions, emotions, thoughts, and behaviour. Schizophrenia, which affects more than 1% of the world's population, is characterised by positive, negative, and cognitive symptoms [1]. The development of these symptoms is attributed to the changes in the levels of intracellular cyclic adenosine monophosphate (cAMP) and cyclic guanosine monophosphate (cGMP), as well as phosphorylation of the cAMP response element binding protein (CREB) [2]. Moreover, dysregulation of the dopamine system, particularly within the prefrontal cortex and striatal network of the basal ganglia, involving the mesolimbic and mesocortical pathways, is also implicated in the pathophysiology of schizophrenia [3,4]. Within this context, the involvement of dopamine (D_1) receptors on striatal neurons contributing to the direct pathway and D_2 receptors on striatal neurons contributing to the indirect pathway plays a significant role in the cascading processes of thalamic disinhibition and inhibition. These mechanisms are associated with the manifestation of psychosis, motor abnormalities, and cognitive impairment [5]. Therefore, the positive symptoms develop due to the hyperactivity of D_2 receptors and the disruption of the cortical network within the nucleus accumbens. While the negative symptoms arise from the decreased function of the nucleus caudatus and reduced stimulation of D_1 receptors in the prefrontal cortex [6].

The mainstay of schizophrenia treatment is typical and atypical antipsychotics having D_2 receptor antagonist effects. However, the D_2 receptor blockers often do not address the negative symptoms and cognitive deficits [7]. Moreover, typical antipsychotics are associated with extrapyramidal side effects due to decreased dopaminergic output of basal ganglia [8,9]. Hence, there is an unmet need for novel approaches beyond dopamine receptor antagonism. These approaches aim not only to enhance the management of positive and negative symptoms but also to address the cognitive impairments associated with schizophrenia, all while reducing the unwanted side effects of the existing treatments [10].

The function of phosphodiesterase (PDE) 1B and PDE10A as dual-substrate regulators of second messenger signalling has been recognised as promising therapeutic targets for treating schizophrenia due to their high expression in the striatum and cortex with vast dopamine and glutaminergic innervations [11,12]. Inhibition of PDE1B and PDE10A results in increased levels of cyclic nucleotides and enhanced phosphorylation of CREB and dopamine- and cyclic-AMP-regulated phosphoprotein (DARPP-32) [13,14]. This presents a promising opportunity for developing therapeutic compounds that specifically target the dopamine- and glutamate-mediated signalling pathways that are impaired in schizophrenia. It has been hypothesised that the PDE1B enzyme is involved in the D_1 receptor inactivation pathway, whereas the PDE10A contributes to the enhanced D_2 receptor activation [15]. Thus, PDE1B inhibitors are notably suitable to manage negative symptoms and cognitive deficits related to schizophrenia through D_1 receptor activation [16]. On the other hand, the PDE10A inhibitors closely mimic D_2 receptor antagonists by disinhibiting the striatopallidal medium spiny neurons (MSNs) that express D_2 [17,18]. Therefore, dual inhibitors of PDE1B and PDE10A that specifically modulate striatal signalling cascades serve as a novel approach for treating the positive, negative, and cognitive symptoms via potentiation of D_1 receptor signalling and suppression of D_2 receptor signalling [19,20].

Recently, *in silico* techniques have received significant attention due to their pivotal role in the drug discovery process, facilitating cost-effective identification of potent drug candidates and promising targets across various diseases. The use of diverse computational approaches such as pharmacophore modelling, virtual screening, and molecular docking has greatly contributed to the identification of potential drug candidates from extensive databases. Furthermore, understanding the three-dimensional (3D) structure of proteins and their interactions with ligands is crucial for discovering novel drugs [21–23]. Accordingly, the present study aims to identify a dual inhibitor of PDE1B and PDE10A through pharmacophore-based screening and molecular docking approaches, followed by structural modification of the lead compound to design novel dual inhibitors of PDE1B and PDE10A with promisingly high activity.

2. Materials and methods

2.1. Databases, software, and servers

ChemDraw Professional 15.0 (PerkinElmer), Protein Data Bank (RCSB PDB), LigandScout 4.4, DecoyFinder 2.0, ChEMBL database, Universal Natural Product Database (UNPD), DruLiTo software, Pan Assay Interference Compounds (PAINS)-Remover server, SwissADME, pkCSM, ProTox-II, Autodock Vina 1.2.0, Discovery Studio (DS) visualizer 2017.

2.2. Ligand-based pharmacophore model development

In a set of active compounds, the spatial configuration of the chemical features is associated with their corresponding activities. A pharmacophore region of a compound is responsible for its biological action, and this model explains how structurally diverse compounds can bind to a common receptor site. The selection of active compounds for constructing the training set, which is used to build the ligand-based pharmacophore model, has a significant impact on the quality of the developed model. Therefore, a thorough literature search was conducted to obtain potent ligands with diverse chemical structures. The following criteria were used to select the training set ligands [1]: the chemical structures of the compounds should be diverse [2]; the IC_{50} of the compounds should be $\leq$ 100 nM [3]; include compounds with the lowest IC_{50} value, and [4] avoid inactive compounds [24]. Conversely, the test set was employed to evaluate the performance of the generated pharmacophore model. It comprises active compounds with well-established direct interactions with the target receptor [25].

The generation of the ligand-based pharmacophore model began with the creation of two-dimensional (2D) structures for the

training set compounds, using ChemDraw 15.0. Subsequently, the compounds were imported into LigandScout 4.4 (Ligand-Based Modelling Perspective) and subjected to energy minimisation using the Merck Molecular force field (MMFF94). Multiple conformations were generated for each compound using iCon BEST settings. Then, the compounds were subjected to clustering based on their similarity in 3D pharmacophore characteristics. Finally, a merged feature pharmacophore model was generated for each cluster [24].

2.3. Pharmacophore validation and refinement

In order to assess the performance of the developed model, the generated pharmacophore model with the highest fit score was selected and validated by screening a library comprising both active (test set) and inactive (decoy set) compounds. Using DecoyFinder 2.0, target-specific decoy sets of PDE1B and PDE10A were created, with a maximum of 50 Da standard deviation from the active ligands, by filtering the ChEMBL database (which contains 8.9 million drug-like compounds) [26].

Automatic clustering of hits such that all the comparable compounds are assembled to retrieve structurally distinct molecules. This approach ensures that both the training and test sets adequately cover the entire descriptor space of the dataset, preventing significant dissimilarity in chemical domains between the two sets. Data splitting assures that each member of the test set is close to at least one point in the training set. The training and test sets should meet the following criteria [1]: representative points in the test and training sets should be close to each other, and [2] the training set should be diverse [27]. It is suggested that the external test set include at least five compounds, representing the full range of descriptors and activity of the compounds in the training set [28]. This split guarantees the model has sufficient data for learning while retaining enough for unbiased testing (Tables 1 and 2).

Several quality indicators were employed to assess the performance of the developed pharmacophore models. These included the yield of actives (percentage of active compounds in the hit list), enrichment factor (enrichment of active molecules compared to random selection), specificity (ability to exclude inactive compounds), sensitivity (ability to identify active molecules), area under the curve of the receiver operating characteristic plot AUC-ROC, as well as the goodness of hit Güner-Henry (GH) score (quantification of model selectivity, coverage of activity space from database screening, accuracy of hits, and recall of actives) [29].

$$EF = \frac{Ha \times D}{Ht \times A}$$

$$GH = \left[\left(\frac{Ha\,(3A + Ht)}{4\,Ht\,A}\right) \times \left(1 - \frac{Ht - Ha}{D - A}\right)\right]$$

EF: Enrichment factor; Ha: Number of actives in the hit list; Ht: Number of hits;
A: Number of actives in the database; D: Number of compounds in the database.

2.4. Sequential virtual screening

The Universal Natural Product Database (UNPD), comprising 228,247 compounds, was used for ligand-based virtual screening to retrieve novel scaffolds with PDE1B and PDE10A inhibition [30,31]. A 3D multi-conformational database in ldb format was created from the molecule library using the ldbgen technique in the Ligand-Based Modelling Perspective of LigandScout, which computes and annotates each conformation with pharmacophore characteristics. Virtual screening was initiated using the validated PDE1B pharmacophore model as a 3D query to retrieve structurally diverse compounds that match the appropriate pharmacophoric features [32]. The obtained hits were ranked based on their pharmacophore fit score (PFS), in which the higher-ranked ones fitted better to the PDE1B-pharmacophore model and were anticipated to be more active than the lower-scoring compounds.

Subsequently, the drug-likeness analysis was performed, in which modified criteria of Lipinski's rule of 5 (RO5) were used to retrieve central nervous system (CNS) active compounds. The modified criteria include retention of compounds with molecular weight < 450 Da, log P 2–5, hydrogen bond donor (HBD) < 3, hydrogen bond acceptor (HBA) < 10, rotatable bonds < 10, and topological polar surface area (TPSA) < 60 Å [33,34]. These criteria were calculated using the DruLiTo software, which provides a comprehensive set of tools for analysing and filtering compounds based on established pharmacokinetic rules. Then, the blood-brain barrier (BBB) likeness filter in the DruLiTo software was employed to ensure the BBB penetration ability. According to the BBB criteria, retained compounds should have a molecular weight of $\leq$400 Da, a total hydrogen bond $\leq$8, and no acids [35].

In the following stage, the filtered hits were subjected to the Pan Assay Interference Compounds (PAINS)-Remover server to remove the false positive compounds that might interfere with the protocol [19]. Finally, the last stage of the virtual screening involved using

Table 1
Allocation of training and test set for PDE1B inhibitors.

Cluster ID	Training	Test
1	1	0
2	0	1
3	3	2
4	1	1
5	2	1
6	4	3
Total	11	8

Table 2
Allocation of training and test set for PDE10A inhibitors.

Cluster ID	Training	Test
1	1	0
2	1	0
3	1	0
4	0	1
5	0	1
6	1	0
7	0	1
10	1	0
11	2	0
12	1	1
13	4	0
14	2	1
15	1	2
16	2	0
17	3	0
18	2	0
19	2	0
20	3	2
Total	29	9

the validated PDE10A pharmacophore model as a 3D query to obtain potential dual inhibitors [36].

2.5. Evaluation of drug-likeness and ADMET properties by computational analysis

The structure of a compound determines its physical and chemical characteristics as well as its ADMET (absorption, distribution, metabolism, excretion, and toxicity) properties. In this study, the physicochemical characteristics and ADMET properties of the retrieved hits were studied using the SwissADME, pkCSM, and ProTox-II to evaluate the pharmacokinetics of the compounds and eliminate toxic ones. [72–75] Each of the five parameters of the ADMET depends on certain factors such as membrane permeability, P-glycoprotein substrate or inhibitor, CNS permeability, CYP450 substrate or inhibitor, total clearance, and organ toxicity. These parameters were determined and checked for compliance with their standard ranges [37–39].

2.6. Molecular docking study

Compounds obtained through virtual screening were subjected to molecular docking studies to determine their optimal orientation within the active sites of the receptors and analyse the interactions responsible for the binding. Autodock Vina 1.2.0 was used to perform molecular docking and identify the compound with the highest affinity for PDE1B and PDE10A [40]. The first step in a successful docking study is the identification of the most appropriate protein structure from the Protein Data Bank (PDB). The criteria of protein selection include high resolution, completeness of the active site and side chains, and the presence of a co-crystallised ligand within the active site [41].

Using AutoDock Tools 1.5.6 (ADT), the selected protein structures were subjected to extraction of co-crystallised ligands, elimination of water molecules, addition of hydrogens and Gasteiger charges, and optimisation of the initial configurations. Subsequently, the ligands were imported into AutoDock, where they were prepared for docking by adding charges, setting the rotatable bonds, and allowing all the torsions to rotate for the ligands. Exhaustiveness was set to 9 to increase the comprehensiveness of the search and the probability of good results. Moreover, the location of the grid box was determined based on the coordinate information of the active site and the atoms of the co-crystallised ligand; thus, the grid box encompasses the active site completely. The molecular docking process started with the re-docking of the co-crystallised ligand into the target receptor, serving as a validation step for the docking protocol. Then, the standards and hits were consecutively subjected to the docking procedure.

2.6.1. Structure-based ligand alignment

Several 3D methods have been developed to align small ligand molecules. These methods are based on three different principles, including molecular interaction field-based, pharmacophore-based, and shape-based alignment methods. Among them, the shape-based alignment method become particularly popular in recent studies [42]. This method seeks to maximise the shape overlap between small molecules. Accordingly, the Discovery Studio (DS) visualizer was used to achieve alignment among the co-crystallised ligand, standard, and top-ranked ligand in a manner that reflects their binding configurations within the receptor. This approach facilitated an in-depth investigation of the ligands' overlap and orientation within the active sites of PDE1B and PDE10A.

2.6.2. Analysis of protein-ligand interactions

The results of the docking study were analysed using the DS visualizer. A comprehensive analysis of protein-ligand interactions was conducted to identify the essential amino acids responsible for the binding of the ligands to the target receptors, PDE1B and PDE10A.

2.7. Design of novel dual inhibitors of PDE1B and PDE10A

The compound with the highest binding affinity for both proteins and appropriate pharmacokinetic parameters was selected as the lead compound. Structural modifications of the lead compound were then proposed as part of a structure-activity-relationship (SAR) study, aimed at designing novel dual inhibitors targeting both PDE1B and PDE10A. The designed inhibitors incorporated functional groups that improved the interactions with the crucial amino acid residues, thus enhancing their affinity for both PDE1B and PDE10A.

3. Results and discussion

3.1. Ligand-based pharmacophore model development

The pharmacophore model depicted the 3D configuration of the chemical features essential for interacting with the target enzymes and producing the desired biological effect [43]. In the ligand-based methodology, the common structural features of the structurally diverse ligands, including HBD, HBA, aromatic ring (AR), hydrophobic area (HA), and exclusion volume (XVOL), were employed to describe the chemical functionalities. Based on the inclusion criteria, the PDE1B-training set comprised 11 active compounds with IC_{50} ranging from 0.06 nM to 70 nM for PDE1B (Table S1). Whereas, 29 compounds with an IC_{50} range of 0.008 nM–64 nM for PDE10A were selected to constitute the PDE10A-training set (Table S2). On the other hand, the PDE1B-test set included eight compounds ($IC_{50} \leq 70$ nM, Table S3), while the PDE10A test set involved nine compounds (IC_{50} 0.42 nM–92 nM Table S4), which were employed to evaluate the developed pharmacophore models.

For each target, ten ligand-based pharmacophore models were generated, in which the model with the highest fit score was considered the best model. As a result, the best pharmacophore model for PDE1B consisted of two HA, two HBA, and 17 XVOL (Fig. 1A), while the best PDE10A pharmacophore model comprised one hydrophobic area, one AR, one HBA, and 11 XVOL (Fig. 1B).

3.2. Pharmacophore validation and refinement

The selected pharmacophore model for each target was refined first by either increasing or decreasing the tolerance radius, feature weight, and exclusion volumes to improve the specificity and sensitivity. Then, the ability of the refined pharmacophore models to identify the active compounds was evaluated using the test set and decoy set validation method. Regarding PDE1B, the developed pharmacophore model was screened against a library of eight actives and 319 decoys. Whereas the screening library used to evaluate the performance of PDE10A-pharmacophore included nine actives and 269 decoys.

The two refined pharmacophore models resulted in high AUC values of the ROC plots, 0.87 for PDE1B (Fig. 2A) and 0.88 for PDE10A (Fig. 2B). These results indicate the reliability of both models in identifying the actives from the decoys, which is attributed to their ability to cover most of the test set compounds and discard the inactive ones. Moreover, the AUC values were higher than 0.5, demonstrating the pharmacophore models' ability to prevent inconsistent randomised selections [44]. Sensitivity and specificity of both models were also high, 0.75 and 0.99 for PDE1B and 0.78 and 0.98 for PDE10A, respectively. This indicates the ability of the developed pharmacophore models to distinguish the active compounds from the inactive decoys. Additionally, the GH scores for both models were high, 0.82 for PDE1B and 0.71 for PDE10A, proving the capability of both models to recognise the true positives, making them optimal pharmacophore models for virtual screening (Table 3) [17,18,45].

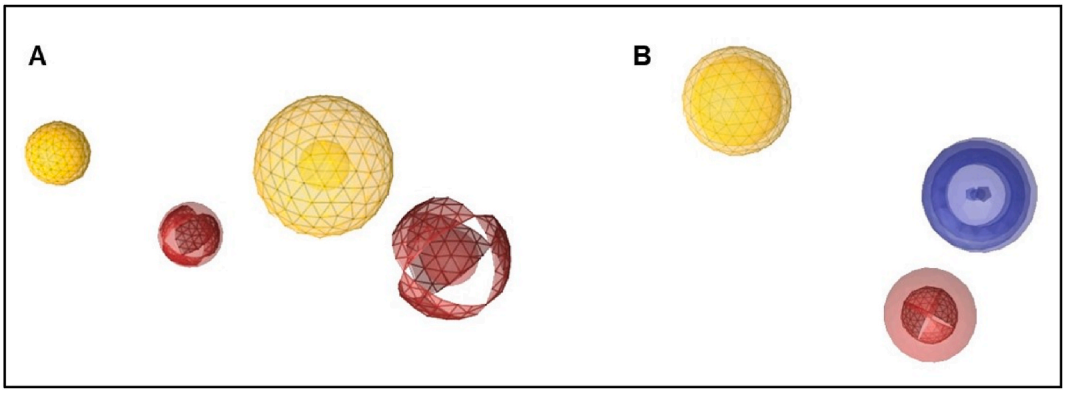

Fig. 1. The ligand-based pharmacophore model. (A) PDE1B-pharmacophore model. (B) PDE10A-pharmacophore model. The pharmacophore features are colour-coded: yellow sphere represents hydrophobic area (HA), red sphere represents hydrogen bond acceptor (HBA), blue sphere represents aromatic ring (AR). (For interpretation of the references to colour in this figure legend, the reader is referred to the Web version of this article.)

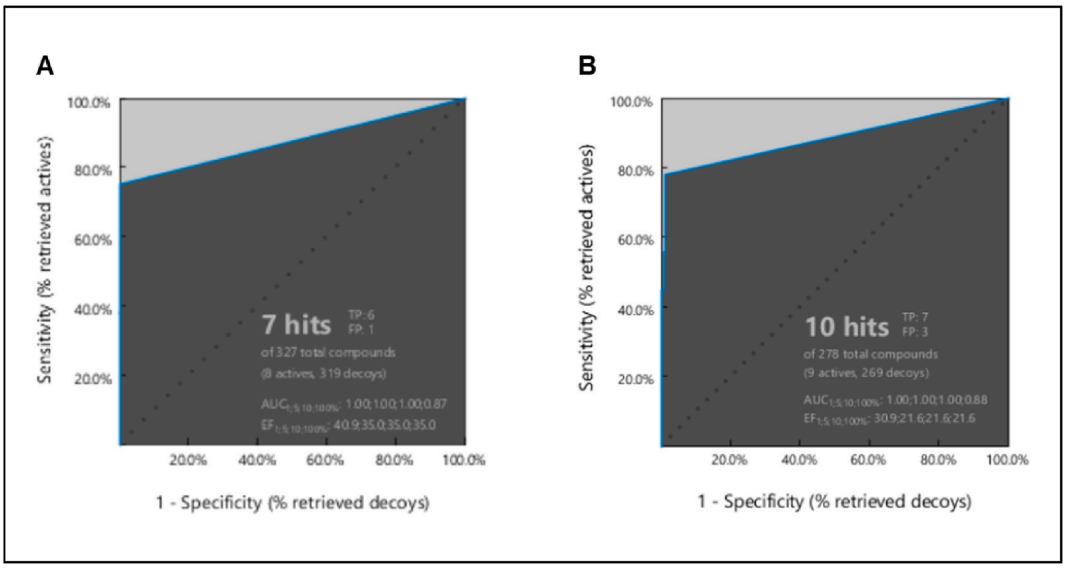

Fig. 2. ROC plots for (A) PDE1B, and (B) PDE10A.

Table 3
Validation results of PDE1B and PDE10A pharmacophore models.

Models	Hits	%Y	ROC	FN	FP	Se	Sp	EF	GH
PDE1B	7	85.71	0.87	2	1	0.75	0.99	35.00	0.82
PDE10A	10	70	0.88	2	3	0.78	0.98	21.62	0.71

*%Y: Yield of actives; FN: False negative; FP: False positive; Se: Sensitivity; Sp: Specificity; EF: Enrichment factor.

3.3. Sequential virtual screening

A total of 3434 hits were obtained after the initial screening. Those hits showed a fit score (PFS) > 45 for PDE1B pharmacophoric features. The number of hits was narrowed down according to Lipinski's RO5 filter, resulting in 647 drug-like hits with a high potential of being orally bioavailable. Subsequently, the BBB filter was applied to retain compounds with high BBB penetrability, resulting in 564 hits. Then, the PAINS-Remover server was used to remove false positive compounds, which included protein-reactive substances that interfered with assay signals or binding interactions by forming aggregates [19]. Based on this filter, 537 hits were obtained. These hits served as the screening database for the PDE10A pharmacophore model, where four hits were retrieved based on the similarity to the PDE10A pharmacophoric features (Fig. 3).

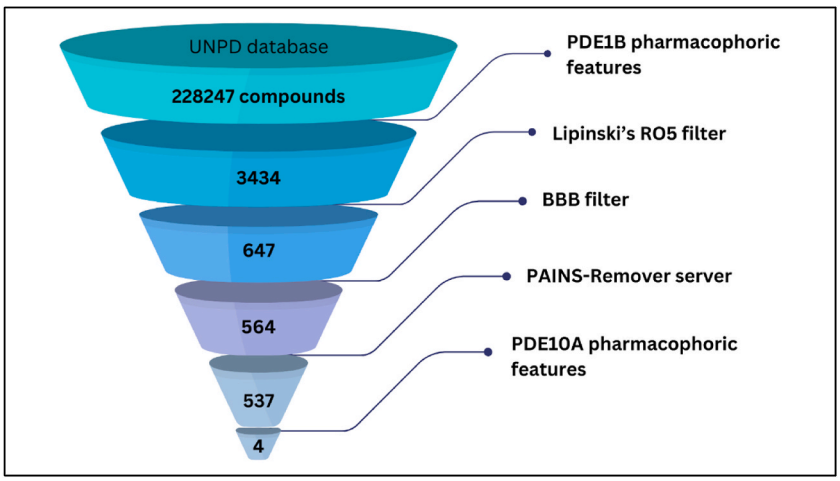

Fig. 3. The sequential workflow for virtual screening of the UNPD.

3.4. Evaluation of drug-likeness and ADMET properties

3.4.1. Drug-likeness analysis

SwissADME was used to predict the physicochemical properties of the four hits that passed all the screening filters (Table S5). The results revealed that the molecular weights of the four compounds were < 400 Da, suggesting their potential for efficient transportation, dispersion, and absorption. Moreover, the compounds displayed ideal lipophilicity (log P 2–5), indicating their appropriate absorption and distribution due to the lipid nature of the cell membrane. Additionally, the TPSA is associated with the compound's absorption properties. The TPSA of the compounds were < 60 Å, suggesting that the compounds have good oral absorption and membrane permeability.

3.4.2. Evaluation of ADMET properties

The ideal oral drug exhibits a combination of essential characteristics including efficient absorption from the gastrointestinal tract, precise distribution to the target site, metabolised without losing its properties, and safe elimination without damage. The dynamic movements of the chemical compounds as they pass through the body and their correlation with various physiological parameters assist us in understanding the pharmacokinetic parameters. To understand these parameters, water solubility, Caco (colon cancer cell line)-2 permeability, intestinal absorption, and P-glycoprotein substrate or inhibitor were computed to predict the absorption level of the compounds.

All compounds were found to be either moderately or poorly soluble in water. CaCo-2 permeability value for all compounds was > 0.9, indicating high permeability and absorption. Moreover, their intestinal absorption values were > 90%, indicating high absorption. Regarding P-glycoprotein, which is a member of the ATP-binding transmembrane glycoprotein family that eliminates drugs and exogenous chemicals from cells, all the compounds were not substrates of P-glycoprotein. Compounds UNPD167314 and UNPD222989 were found to be P-glycoprotein I inhibitors, while compound UNPD222989 was found to be the only P-glycoprotein II inhibitor.

Few parameters were considered to characterise the distribution of compounds. One of these parameters was the distribution volume (VDss), which is a pharmacokinetic parameter that indicates the tendency of the drug to distribute in various tissues *in vivo*. A low volume of distribution (log VDss < − 0.15) indicates that the drug tends to remain in the plasma, while a high value (log VDss > 0.45) indicates that the drug has the tendency to exit the plasma and pass into the extravascular compartments. Accordingly, the results showed that the distribution volume of the compounds was moderate, in which their values were > − 0.15 and < 0.45. In addition, all the compounds were predicted to be able to cross the BBB easily (logBB ≥ 0.3), except UNPD176347 with logBB 0.21, and penetrate the CNS (logPS is > -3).

The Cytochrome P450s (CYP) enzyme system plays a pivotal role in the metabolism of drugs within the liver. Among these enzymes, CYP2D6 and CYP3A4 are the two main subtypes. For metabolism parameters, the results indicated that none of the compounds were a substrate for CYP2D6. Compounds UNPD170560, UNPD222989, and UNPD176347 were substrates for CYP3A4. The four compounds were predicated to be CYP1A2 and CYP2C19 inhibitors. However, only compounds UNPD222989 and UNPD176347 were anticipated to be CYP2C9 inhibitors, while compound UNPD167314 was predicted to be a CYP3A4 inhibitor. This suggested that all the compounds, except UNPD167314, may be metabolised in the liver. Moreover, the elimination of the drug from the body is related to the hydrophilicity of the compound and the molecular weight. The pkCSM results predicted that all compounds showed high values of clearance, where the total clearance of UNPD222989 was the highest, followed by UNPD176347, UNPD167314, and UNPD170560.

The ProTox-II model suggested that compounds UNPD167314 and UNPD222989 toxicity would be class III (moderately toxic), with an LD50 value of 50–300 mg/kg. Whereas, compounds UNPD170560 and UNPD176347 toxicity would be class V (slightly toxic), with an LD50 value of 300–2000 mg/kg. Furthermore, compounds UNPD167314 and UNPD170560 were inactive for Hepatotoxicity, carcinogenicity, mutagenicity, and cytotoxicity, indicating they are not acutely toxic. However, compounds UNPD222989 and

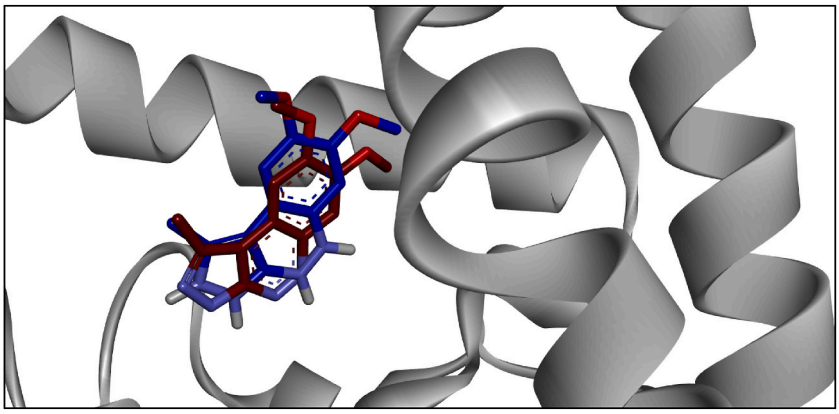

Fig. 4. Superimposed structures of the co-crystallised ligand JY4 (red) over the docked pose (blue), RMSD = 0.22 Å. (For interpretation of the references to colour in this figure legend, the reader is referred to the Web version of this article.)

UNPD176347 were active for mutagenicity.

3.5. Molecular docking study

The 3D crystal structures of PDE1B (PDB ID: 5UP0) and PDE10A (PDB ID: 6MSA) with a resolution of 2.04 Å and 2.06 Å, respectively, were obtained from the PDB. DSR-141562, a known PDE1B inhibitor with an IC_{50} of 43.9 nM, and TAK-063, a selective and potent PDE10A inhibitor with an IC_{50} of 0.3 nM, were used as the standard compounds to facilitate comparison of binding affinity with the obtained hits [46–51]. Initially, the accuracy of the docking protocol was assessed by redocking the PDE10A-co-crystallised ligand, JY4, into the active site of PDE10A. The JY4 was superimposed on its docked pose to determine the RMSD between the two ligands. As a result, the produced RMSD value between the generated pose of the docked ligand and the original one was found to be 0.22 Å, indicating the capability of the docking protocol to reproduce the original pose (Fig. 4). Then, the standards and the four obtained hits were docked into the active site of PDE1B and PDE10A structures, and subsequently ranked based on their docking scores and favourable interactions (Table 4).

The binding site architecture of PDE1B and PDE10A exhibit significant similarity, meeting all the required criteria for a druggable binding site. This site consists of a metal binding pocket, known as the M pocket, an area containing important divalent metal ions (Zn^{2+} and Mg^{2+}) crucial for catalysing the hydrolysis of cAMP and cGMP. In addition, it includes a solvent-filled side pocket with polar residues and the Q pocket, known as the inhibitor pocket. The Q pocket is further divided into the conserved aromatic hydrophobic clamp, known as the P-clamp, and invariant substate-recognising glutamine. The P-clamp comprises an aromatic PHE (PHE424 in PDE1B vs PHE729 in PDE10A) located at the roof of the P-clamp; and two hydrophobic residues, LEU388 and PHE392 in PDE1B vs ILE692 and PHE696 in PDE10A, located on the floor of the binding site [17]. The "glutamine switch" hypothesis was demonstrated by the hydrogen bonding with GLN421 in PDE1B and GLN726 in PDE10A at the nucleotide-binding sites, facilitating dual substrate-specificity and stringent selection of both cAMP and cGMP. Consequently, an effective scaffold for a PDE inhibitor should include a planar ring structure positioned between the P-clamp residues and forming hydrogen bonds with the polar residue GLN, thus optimising its binding and inhibitory potential.

The docking results showed that all the compounds exhibited sufficient affinity for the target proteins (binding affinity $<$ -6.5 kcal/mol). However, UNPD167314 has shown the highest binding affinity for both PDE1B (−8.4 kcal/mol) and PDE10A (−9.7 kcal/mol). Thus, flexible alignment of UNPD167314 with DSR-141562 and the PDE1B co-crystallised ligand (8HP) was performed (Fig. 5A, B, 5C). The results revealed an overall good overlap (Fig. 5D). Interestingly, UNPD167314 and DSR-141562 exhibited a similar orientation to 8HP, suggesting the potential for UNPD167314 to interact with PDE1B in a similar manner to 8HP and DSR-141562, implying the possibility of similar inhibitory effects. In detail, the quinoline group of UNPD167314 and the trifluoromethyl-cyclohexane moiety of DSR-141562 showed the same orientation as the dihydrotriazolo-pyrimidinone moiety of 8HP, occupying the P-clamp and forming hydrophobic interactions with LEU388, PHE392, and PHE424, except UNPD167314 which interacted only with LEU388 and PHE424 (Fig. 6A, B, 6C). In addition, the dihydroindolizinone moiety of UNPD167314 closely aligned with the methoxy-imidazole-triazinone of DSR-141562, both demonstrating Pi-metal interactions with HIS223. Moreover, the tetrahydropyran moiety of DSR-141562 and tetrahydrobenzo-thiophene moiety of 8HP engaged in aromatic interactions with MET336. All three ligands established hydrogen bonds with the residues in the PDE1B active site. Specifically, 8HP formed two bonds with HIS373 and one bond with GLN421, DSR-141562 formed two bonds with TYR222 and GLN421, and UNPD167314 formed one bond with HIS267. DSR-141562 was the only ligand that exhibited two halogen interactions with SER420. Based on the docking results, all the ligands interacted with the main residues that formed the P-clamp, LEU388, PHE392 and PHE424, exhibiting sufficient affinity for PDE1B. However, 8HP demonstrated the highest affinity, primarily attributed to the additional aromatic interactions it formed with MET389, LEU409, and VAL417.

In regard to PDE10A, the quinoline group of UNPD167314, the dimethoxybenzene moiety of JY4, and the fluorophenyl pyrazole of TAK-063 occupied the P-clamp (Fig. 5E, F, 5G) and engaged in interactions with the hydrophobic residues ILE692, PHE696, and PHE729 (Fig. 6D, E, 6F). In addition, the dihydroindolizinone moiety of UNPD167314 closely aligned with the methoxy-pyridazinone of TAK-063 (Fig. 5H), both exhibiting Pi-metal interactions with HIS525. However, the methyl-dihydropyrazole moiety of JY4 established aromatic interaction with HIS525. Notably, both JY4 and TAK-063 formed hydrogen bonds with the residues in the

Table 4
Molecular docking results for PDE1B and PDE10A.

Ligand	Binding affinity with PDE1B (kcal/mol)	Binding affinity with PDE10A (kcal/mol)
8HP[a]	−9.4	
JY4[b]		−8.1
DSR-141562[c]	−9.1	
TAK-063[d]		−9.0
UNPD167314	**−8.4**	**−9.7**
UNPD170560	−7.2	−8.4
UNPD222989	−7.2	−7.6
UNPD176347	−6.6	−7.0

[a] PDE1B-co-crystallised ligand.
[b] PDE10A-co-crystallised ligand.
[c] PDE1B-standard.
[d] PDE10A-standard.

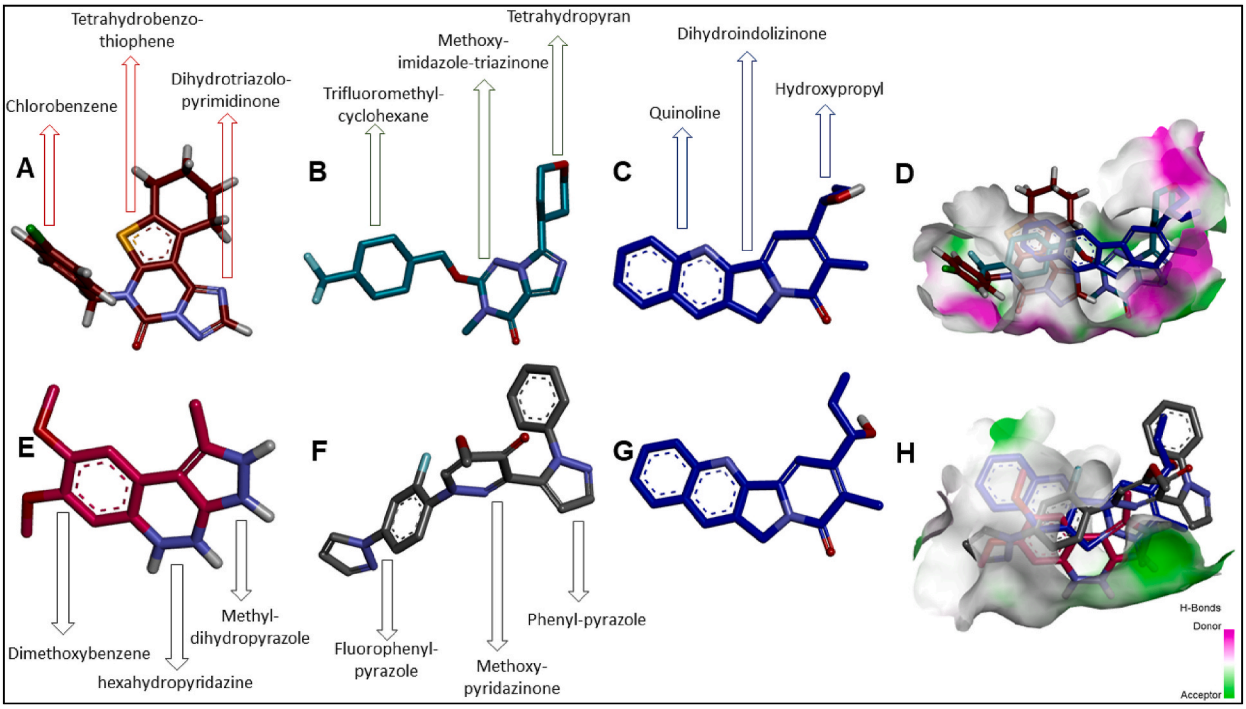

Fig. 5. The orientation of (A) PDE1B-co-crystallised ligand (8HP, red), (B) PDE1B standard (DSR-141562, dark green), and (C) UNPD167314 (dark blue) within the binding site of PDE1B. (D) Mapping surface showing the ligands occupying the active pocket of PDE1B. The orientation of (E) PDE10A-co-crystallised ligand (JY4, pink), (F) PDE10A standard (TAK-063, olive green), and (G) UNPD167314 (dark blue) within the binding site of PDE10A. (H) Mapping surface showing the ligands occupying the active pocket of PDE10A. (For interpretation of the references to colour in this figure legend, the reader is referred to the Web version of this article.)

PDE10A active site. Specifically, JY4 established three bonds with ASP674 and one bond with TYR524, while TAK-063 formed one bond with HIS525.

3.6. Design of novel selective PDE1B and PDE10A inhibitors

Based on the extensive assessment of the physicochemical properties, pharmacokinetic parameters, docking scores, and protein-ligand interactions of the obtained hits, UNPD167314 fulfils all the prerequisites for an effective PDE inhibitor. The scaffold of UNPD167314 includes indole and quinoline moieties, which have extensive biological activities and various pharmaceutical and medical applications. Several natural and synthetic compounds with either indole or quinoline scaffold are available, such as Serotonin (vasoconstrictor hormone), Bufotenine (hallucinogenic agent), Ferroquine (antimalarial), and Dactolisib (antitumor). Additionally, indole shows antimicrobial, anti-inflammatory, anticancer, antihypertensive, antidiabetic, and antioxidant properties, while quinoline exhibits antibacterial, antiparasitic, antiviral, anti-Alzheimer, anticholesterol, and anticancer activities [52–56]. The combinations of these fused heterocyclic structures can result in the development of novel polycyclic frameworks with the most diverse physical, chemical, and biological properties. Therefore, UNPD167314 has been selected as a lead molecule for designing dual inhibitors targeting PDE1B and PDE10A, with higher affinities than the initial lead compound. The SAR of the UNPD167314 scaffold was evaluated to identify the essential functional groups responsible for binding and affinity, as well as the potential substituents to enhance the binding affinity.

According to the binding mode of UNPD167314 within the active site of PDE1B and PDE10A, the quinoline and dihydroindolizinone moieties were kept as these groups are essential for activity and retaining the hydrophobic interactions with the P-clamp residues. As a consequence, the structural refinements were targeted toward R_1 para-substitution of the quinoline ring to improve hydrophobic interactions as well as R_2 carbonyl of the dihydroindolizinone and R_3 hydroxy of the hydroxypropyl to increase hydrogen bonding opportunities. A total of 35 novel inhibitors were designed based on the structural modifications of UNPD167314 (Table S6).

The R_1 position was explored to study the para-substitution of the quinoline ring in order to enhance the hydrophobic interactions of the lead compound with the hydrophobic residues in the P-clamp of PDE1B and PDE10A. The replacement of hydrogen at R_1 with nonpolar lipophilic groups such as phenyl, tertbutyl, and 2-fluoropropan-2-yl significantly enhanced the binding affinity towards both proteins. Among all, tertbutyl substitution resulted in the highest binding affinity with an average binding affinity of $<$ -10.8 kcal/mol. The high affinity of the compounds with tertbutyl substituent can be attributed to the large size of the tertbytyl group and its adequate lipophilicity, followed by phenyl and 2-fluoropropan-2-yl, respectively. On the other hand, the hydrogen substituent in the R_1 position

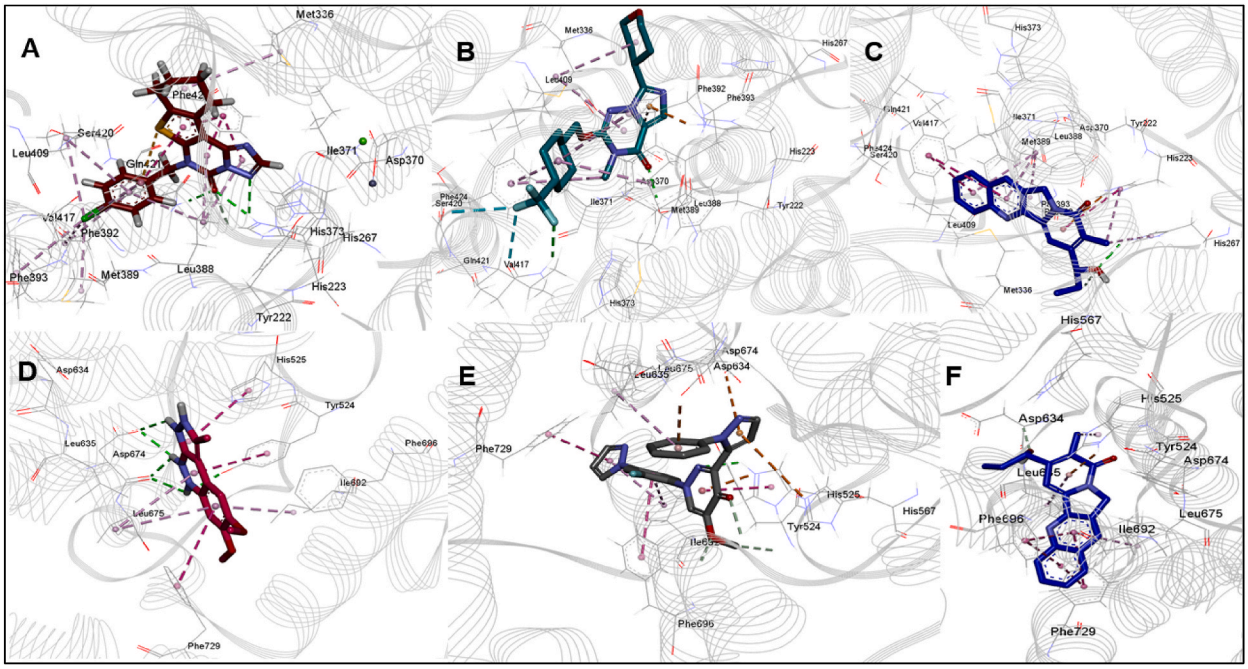

Fig. 6. 3D representation of the protein-ligand interactions. Interactions of (A) PDE1B-co-crystallised ligand (8HP, red), (B) PDE1B standard (DSR-141562, dark green), and (C) UNPD167314 (dark blue) with PDE1B. Interactions of (D) (JY4, pink), (E) PDE10A standard (TAK-063, olive green), and (F) UNPD167314 (dark blue) with PDE10A. The interactions are colour-coded: Green: Hydrogen bond, Pink: Aromatic interaction, Orange: Pi-metal interaction, and Cyan: Halogen interaction. (For interpretation of the references to colour in this figure legend, the reader is referred to the Web version of this article.)

led to a decreased binding affinity, primarily attributed to reduced binding interactions with key residues. This indicates that tertbutyl proved to be optimal in this position compared to smaller groups, allowing more hydrophobic contacts with the P-clamp, along with deeper insertion and a tighter fit within the active sites.

The modifications made at the R_2 and R_3 positions aimed to improve the hydrogen bonding opportunities. Polar hydrophilic groups with the potential of forming hydrogen bonds were substituted at these positions. The carbonyl group at the R_2 position was substituted with hydroxy and methoxy groups, respectively. As a result, the hydroxy substituent increased the binding affinity compared to the methoxy substituent. This could be attributed to the higher electronegativity of the hydroxy group compared to the methoxy group. In addition, the methoxy substituent imposed significant steric hindrance, resulting in a slightly lower binding affinity.

In regard to R_3, the hydroxy group at this position was replaced with carbonyl and carboxy groups, respectively. The introduction of the carboxyl group enhanced the binding affinity via additional hydrogen bonding interactions. This enhancement was attributed to the highly polar nature of the carbonyl and hydroxy groups, which served as hydrogen bond acceptors and donors simultaneously, thereby facilitating hydrogen bonding. As a result, there was a significant increase in hydrogen bonding interactions observed with GLN421, HIS296, HIS267, and HIS223 in PDE1B, as well as GLN726, TYR693, and PHE729 in PDE10A.

Among the 35 designed compounds, seven compounds (compound 9, 10, 12, 18, 19, 20, and 21) displayed substantial affinity for PDE1B (binding affinity of −11 kcal/mol), while six compounds (compound 18, 19, 20, 21, 22, and 23) showed high affinity for PDE10A (binding affinity of ≤ -11.2 kcal/mol). Upon examining the structures of these compounds, we noticed that tertbutyl at R_1 position and either carbonyl or hydroxy group at R_2 position are common among them. This observation suggests that these specific groups are well-suited for optimal interactions at R_1 and R_2 positions, contributing to high affinity. Interestingly, only four compounds (compounds 18, 19, 20, and 21) (Fig. 7) exhibited significant and similar affinities for both enzymes (binding affinity of −11 kcal/mol for PDE1B and −11.2 kcal/mol for PDE10A). These compounds hold promise as potential candidates for development as dual inhibitors targeting PDE1B and PDE10A due to their high affinity for both enzymes.

3.6.1. Drug-likeness and ADMET analysis of the designed inhibitors

Generally, compounds 18, 19, 20, and 21 displayed ideal physicochemical properties to achieve the desired BBB permeation, characterised by high lipophilicity (log P < 5) and low molecular weight (< 400 g/mol). These properties aligned with desirable drug-likeness properties, resulting in good oral absorption and membrane permeability (Table S7). Specifically, replacing the hydrogen at R_1 with tertbutyl and introducing either a carbonyl or carboxyl at R_3 to replace the hydroxy significantly enhanced intestinal absorption to 98.94 % and 99.37 % in compounds 19 and 20, respectively, compared to 98.44 % in the lead compound. Moreover, all four compounds contained < 5 rotatable bonds, maintaining structural rigidity. This rigidity is crucial because the larger number of rotatable bonds can lead to a flexible structure of the inhibitor, converting the active conformation to inactive that fails to interact

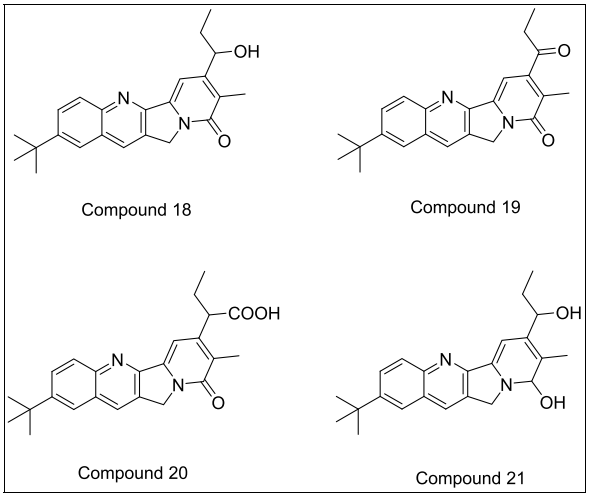

Fig. 7. Structures of the designed compounds with high affinity for PDE1B and PDE10A.

effectively with PDE1B and PDE10A, potentially causing unwanted interactions with other receptors and side effects. Additionally, the synthetic accessibility scores slightly increased due to structural modifications but remained below 5, indicating reasonable feasibility in synthesising the newly designed dual inhibitor.

Furthermore, substituting the hydrogen at R_1 with tertbutyl and replacing the carbonyl at R_2 with hydroxy in compound 21 reduced its toxicity. Compounds 18, 19, and 20 showed similar toxicity profiles to the lead. However, compound 21 displayed reduced toxicity, classifying it as Class V (slightly toxic) with an LD50 value of 1000 mg/kg. Notably, all compounds demonstrated inactivity with regard to hepatotoxicity, carcinogenicity, mutagenicity, and cytotoxicity, indicating their non-toxic nature.

4. Conclusions

A computer-aided drug design approach was utilised to identify a lead compound acting as a dual inhibitor of PDE1B and PDE10A and design novel inhibitors with improved properties. The developed compounds aim to alleviate the positive, negative, and cognitive symptoms of schizophrenia, considering the limited effectiveness of current therapies. The approach involved employing ligand-based pharmacophore modelling to reveal essential structural features required for inhibiting PDE1B and PDE10A activity. This was followed by a sequential virtual screening of the UNPD library, integrating drug-likeness filters and ADMET analysis, which yielded four promising hits. These hits were further assessed based on their binding affinities for PDE1B and PDE10A. As a result, UNPD167314 was selected as the lead compound due to its favourable pharmacokinetic properties and high affinity for both targets. Studying the SAR of the lead compound led to the design of 35 novel dual inhibitors based on the structural modification of the UNPD167314 scaffold. Among these, four compounds exhibited comparable binding affinities to PDE1B and PDE10A, where the structures of the four compounds include tertbutyl at the R_1 position. These four compounds showed optimal physicochemical properties and drug-likeness characteristics, making them promising candidates for synthesis and subsequent evaluation using *in vitro* and *in vivo* approaches.

Funding

This research was funded by Centre of Excellence for Research, Value Innovation and Entrepreneurship (CERVIE), UCSI University (Project Code: REIG-FPS-2020/051).

Data availability statement

Data included in article/supplementary material/referenced in article.

Credit author statement

Ching Wen Soon: Performed the experiments; Analyzed and interpreted the data; Wrote the manuscript. Anand Gaurav: Designed the experiments; Obtained the funding; Analyzed and interpreted the data, Reviewed the manuscript. Vertika Gautam: Designed the experiments; Reviewed the manuscript. Mayasah Al-Nema: Analyzed and interpreted the data; Wrote and Reviewed the manuscript.

Declaration of competing interest

The authors declare that they have no known competing financial interests or personal relationships that could have appeared to

influence the work reported in this paper.

Acknowledgements

None.

Appendix A. Supplementary data

Supplementary data to this article can be found online at https://doi.org/10.1016/j.heliyon.2024.e38305.

References

[1] E.P. Knott, M. Assi, S.N. Rao, M. Ghosh, D.D. Pearse, Phosphodiesterase inhibitors as a therapeutic approach to neuroprotection and repair, Int. J. Mol. Sci. 18 (4) (2017) 696.
[2] F.E. Padovan-Neto, S. Sammut, S. Chakroborty, A.M. Dec, S. Threlfell, P.W. Campbell, et al., Facilitation of corticostriatal transmission following pharmacological inhibition of striatal phosphodiesterase 10A: role of nitric oxide-soluble guanylyl cyclase-cGMP signaling pathways, J. Neurosci. 35 (14) (2015) 5781–5791.
[3] H.-T. Zhang, Y. Xu, J.M. O'Donnell, Phosphodiesterases: CNS Functions and Diseases, Springer, 2017.
[4] S.X. Luo, E.J. Huang, Dopaminergic neurons and brain reward pathways: from neurogenesis to circuit assembly, Am. J. Pathol. 186 (3) (2016) 478–488.
[5] E. Perez-Costas, M. Melendez-Ferro, R.C. Roberts, Basal ganglia pathology in schizophrenia: dopamine connections and anomalies, J. Neurochem. 113 (2) (2010) 287–302.
[6] R. Brisch, A. Saniotis, R. Wolf, H. Bielau, H.-G. Bernstein, J. Steiner, et al., The role of dopamine in schizophrenia from a neurobiological and evolutionary perspective: old fashioned, but still in vogue, Front. Psychiatr. 5 (2014) 47.
[7] R. Walker, Clinical Pharmacy and Therapeutics E-Book, Elsevier Health Sciences, 2011.
[8] C.J. Schmidt, D.S. Chapin, J. Cianfrogna, M.L. Corman, M. Hajos, J.F. Harms, et al., Preclinical characterization of selective phosphodiesterase 10A inhibitors: a new therapeutic approach to the treatment of schizophrenia, J. Pharmacol. Exp. Therapeut. 325 (2) (2008) 681–690.
[9] M. Al-Nema, A. Gaurav, Schizophrenia: the ambiguous mechanism behind the disorder, Jordan Journal of Pharmaceutical Sciences 15 (2) (2022) 239–257.
[10] J.A. Siuciak, The role of phosphodiesterases in schizophrenia: therapeutic implications, CNS Drugs 22 (2008) 983–993.
[11] S. Delhaye, B. Bardoni, Role of phosphodiesterases in the pathophysiology of neurodevelopmental disorders, Mol. Psychiatr. 26 (9) (2021) 4570–4582.
[12] M.Y. Al-Nema, A. Gaurav, Phosphodiesterase as a target for cognition enhancement in schizophrenia, Curr. Top. Med. Chem. 20 (26) (2020) 2404–2421.
[13] S. Threlfell, S. Sammut, F.S. Menniti, C.J. Schmidt, A.R. West, Inhibition of phosphodiesterase 10A increases the responsiveness of striatal projection neurons to cortical stimulation, J. Pharmacol. Exp. Therapeut. 328 (3) (2009) 785–795.
[14] M.Y. Al-Nema, A. Gaurav, Protein-protein interactions of phosphodiesterases, Curr. Top. Med. Chem. 19 (7) (2019) 555–564.
[15] T.W. Shy, A. Gaurav, Pharmacophore modelling and virtual screening studies for the discovery of potential natural products based PDE1B inhibitor lead compounds, Cent. Nerv. Syst. Agents Med. Chem. 21 (3) (2021) 195–204.
[16] S. McQuown, S. Xia, K. Baumgärtel, R. Barido, G. Anderson, B. Dyck, et al., Phosphodiesterase 1b (PDE1B) regulates spatial and contextual memory in hippocampus, Front. Mol. Neurosci. 12 (2019) 21.
[17] M. Al-Nema, A. Gaurav, V.S. Lee, B. Gunasekaran, M.T. Lee, P. Okechukwu, et al., Structure-based discovery and bio-evaluation of a cyclopenta [4, 5] thieno [2, 3-d] pyrimidin-4-one as a phosphodiesterase 10A inhibitor, RSC Adv. 12 (3) (2022) 1576–1591.
[18] M. Al-Nema, A. Gaurav, G. Akowuah, Discovery of natural product inhibitors of phosphodiesterase 10A as novel therapeutic drug for schizophrenia using a multistep virtual screening, Comput. Biol. Chem. 77 (2018) 52–63.
[19] M. Al-Nema, A. Gaurav, V.S. Lee, B. Gunasekaran, M.T. Lee, P. Okechukwu, Identification of dual inhibitor of phosphodiesterase 1B/10A using structure-based drug design approach, J. Mol. Liq. 342 (2021) 117485.
[20] M. Al-Nema, A. Gaurav, M.T. Lee, P. Okechukwu, P. Nimmanpipug, V.S. Lee, Evaluation of the acute oral toxicity and antipsychotic activity of a dual inhibitor of PDE1B and PDE10A in rat model of schizophrenia, PLoS One 17 (12) (2022) e0278216.
[21] A. Gaurav, M. Xing, M. Al-Nema, A. Gaurav, M. Xing, M. Al-Nema, Computational approaches in the development of phosphodiesterase inhibitors, Quantitative Structure-activity Relationship (2017) 160–169.
[22] J. Shi, H.-F. Cao, C.-F. Wang, S. Gao, J.-Y. Wang, L.-X. Zhao, et al., In silico approach of novel HPPD/PDS dual target inhibitors by pharmacophore, AILDE and molecular docking, J. Taiwan Inst. Chem. Eng. 143 (2023) 104711.
[23] J.-Y. Wang, S. Gao, J. Shi, H.-F. Cao, T. Ye, M.-L. Yue, et al., Virtual screening based on pharmacophore model for developing novel HPPD inhibitors, Pestic. Biochem. Physiol. 184 (2022) 105109.
[24] G. Wolber, T. Langer, LigandScout: 3-D pharmacophores derived from protein-bound ligands and their use as virtual screening filters, J. Chem. Inf. Model. 45 (1) (2005) 160–169.
[25] T. Kaserer, K.R. Beck, M. Akram, A. Odermatt, D. Schuster, Pharmacophore models and pharmacophore-based virtual screening: concepts and applications exemplified on hydroxysteroid dehydrogenases, Molecules 20 (12) (2015) 22799–22832.
[26] C.M. Adrià, S. Garcia-Vallvé, G. Pujadas, DecoyFinder, a tool for finding decoy molecules, J. Cheminf. 4 (1) (2012) 1.
[27] A. Golbraikh, A. Tropsha, Beware of q2, J. Mol. Graph. Model. 20 (4) (2002) 269–276.
[28] A. Tropsha, P. Gramatica, V.K. Gombar, The importance of being earnest: validation is the absolute essential for successful application and interpretation of QSPR models, QSAR Comb. Sci. 22 (1) (2003) 69–77.
[29] A. Vuorinen, D. Schuster, Methods for generating and applying pharmacophore models as virtual screening filters and for bioactivity profiling, Methods 71 (2015) 113–134.
[30] J. Gu, Y. Gui, L. Chen, G. Yuan, H.-Z. Lu, X. Xu, Use of natural products as chemical library for drug discovery and network pharmacology, PLoS One 8 (4) (2013) e62839.
[31] ISDB by oolonek. Available from::https://oolonek.github.io/ISDB/.
[32] M. Al-Nema, A. Gaurav, V.S. Lee, Docking based screening and molecular dynamics simulations to identify potential selective PDE4B inhibitor, Heliyon 6 (9) (2020) e04856.
[33] H. van de Waterbeemd, G. Camenisch, G. Folkers, J.R. Chretien, O.A. Raevsky, Estimation of blood-brain barrier crossing of drugs using molecular size and shape, and H-bonding descriptors, J. Drug Target. 6 (2) (1998) 151–165.
[34] F. Atkinson, S. Cole, C. Green, H. Van de Waterbeemd, Lipophilicity and other parameters affecting brain penetration, Curr. Med. Chem. Cent. Nerv. Syst. Agents 2 (3) (2002) 229–240.
[35] L. Di, E.H. Kerns, Drug-like Properties: Concepts, Structure Design and Methods from ADME to Toxicity Optimization, Academic press, 2015.
[36] Q. Gao, L. Yang, Y. Zhu, Pharmacophore based drug design approach as a practical process in drug discovery, Curr. Comput. Aided Drug Des. 6 (1) (2010) 37–49.

[37] A.A. Zackria, R. Pattabiraman, T.K. Murthy, S.B. Kumar, B.B. Mathew, V.G. Biju, Computational screening of natural compounds from Salvia plebeia R. Br. for inhibition of SARS-CoV-2 main protease, Vegetos (2021) 1–15.
[38] Y. Han, J. Zhang, C.Q. Hu, X. Zhang, B. Ma, P. Zhang, In silico ADME and toxicity prediction of ceftazidime and its impurities, Front. Pharmacol. 10 (2019) 434.
[39] S. Basnet, M.P. Ghimire, T.R. Lamichhane, R. Adhikari, A. Adhikari, Identification of potential human pancreatic α-amylase inhibitors from natural products by molecular docking, MM/GBSA calculations, MD simulations, and ADMET analysis, PLoS One 18 (3) (2023) e0275765.
[40] G.M. Morris, M. Lim-Wilby, Molecular docking. Molecular Modeling of Proteins, 2008, pp. 365–382.
[41] C. Zardecki, S. Dutta, D.S. Goodsell, M. Voigt, S.K. Burley, RCSB Protein Data Bank: A Resource for Chemical, Biochemical, and Structural Explorations of Large and Small Biomolecules, ACS Publications, 2016.
[42] J. Hu, Z. Liu, D.-J. Yu, Y. Zhang, LS-align: an atom-level, flexible ligand structural alignment algorithm for high-throughput virtual screening, Bioinformatics 34 (13) (2018) 2209–2218.
[43] M. Conti, J. Beavo, Biochemistry and physiology of cyclic nucleotide phosphodiesterases: essential components in cyclic nucleotide signaling, Annu. Rev. Biochem. 76 (2007) 481–511.
[44] N. Triballeau, F. Acher, I. Brabet, J.-P. Pin, H.-O. Bertrand, Virtual screening workflow development guided by the "receiver operating characteristic" curve approach. Application to high-throughput docking on metabotropic glutamate receptor subtype 4, J. Med. Chem. 48 (7) (2005) 2534–2547.
[45] M. Al-Nema, A. Gaurav, V.S. Lee, Designing of 2, 3-dihydrobenzofuran derivatives as inhibitors of PDE1B using pharmacophore screening, ensemble docking and molecular dynamics approach, Comput. Biol. Med. (2023) 106869.
[46] A. Harada, K. Suzuki, N. Kamiguchi, M. Miyamoto, K. Tohyama, K. Nakashima, et al., Characterization of binding and inhibitory properties of TAK-063, a novel phosphodiesterase 10A inhibitor, PLoS One 10 (3) (2015) e0122197.
[47] T. Enomoto, A. Tatara, M. Goda, Y. Nishizato, K. Nishigori, A. Kitamura, et al., A novel phosphodiesterase 1 inhibitor DSR-141562 exhibits efficacies in animal models for positive, negative, and cognitive symptoms associated with schizophrenia, J. Pharmacol. Exp. Therapeut. 371 (3) (2019) 692–702.
[48] RCSB PDB - 5UP0: Crystal structure of human PDE1B catalytic domain in complex with inhibitor 3 (6-(4-chlorobenzyl)-8,9,10,11-tetrahydrobenzo[4,5]thieno [3,2-e][1,2,4]triazolo[1,5-c]pyrimidin-5(6H)-one). Available from: https://www.rcsb.org/structure/5up0.
[49] B. Dyck, B. Branstetter, T. Gharbaoui, A.R. Hudson, J.G. Breitenbucher, L. Gomez, et al., Discovery of selective phosphodiesterase 1 inhibitors with memory enhancing properties, J. Med. Chem. 60 (8) (2017) 3472–3483.
[50] RCSB PDB - 6MSA: Novel, potent, selective and brain penetrant phosphodiesterase 10A inhibitors. Available from:: https://www.rcsb.org/structure/6MSA.
[51] H. Geneste, K. Drescher, C. Jakob, L. Laplanche, M. Ochse, M. Torrent, Novel, potent, selective, and brain penetrant phosphodiesterase 10A inhibitors, Bioorg. Med. Chem. Lett 29 (3) (2019) 406–412.
[52] J. Dhuguru, R. Skouta, Role of indole scaffolds as pharmacophores in the development of anti-lung cancer agents, Molecules 25 (7) (2020) 1615.
[53] N.K. Kaushik, N. Kaushik, P. Attri, N. Kumar, C.H. Kim, A.K. Verma, et al., Biomedical importance of indoles, Molecules 18 (6) (2013) 6620–6662.
[54] P. Yadav, K. Shah, Quinolines, a perpetual, multipurpose scaffold in medicinal chemistry, Bioorg. Chem. 109 (2021) 104639.
[55] L.F. Moor, T.R. Vasconcelos, R. da R Reis, L.S. Pinto, T.M. da Costa, Quinoline: an attractive scaffold in drug design, Mini Rev. Med. Chem. 21 (16) (2021) 2209–2226.
[56] A. Gaurav, M. Al-Nema, Polymerases of coronaviruses: structure, function, and inhibitors. Viral Polymerases, Elsevier, 2019, pp. 271–300.